Scaling functions, self-similarity, and the morphology of phase-separating systems

P. Fratzl
*Departments of Mathematics and Physics, Rutgers University, Busch Campus, New Brunswick, New Jersey 08903 and Institut für Festkörperphysik der Universität Wien, Strudlhofgasse 4, A-1090 Wien, Austria**

J. L. Lebowitz
Departments of Mathematics and Physics, Rutgers University, Busch Campus, New Brunswick, New Jersey 08903

O. Penrose
Department of Mathematics, Heriot-Watt University, Riccarton, Edinburgh EH14 4A5, United Kingdom

J. Amar
Department of Physics, Emory University, Atlanta, Georgia 30322
(Received 29 March 1991)

In the late stages of phase separation in liquids or solids with negligible coherency stresses, the structure function $S(k,t)$ is known to follow a scaling behavior in the form $S(k,t)\sim k_m^{-3}(t)F(k/k_m(t))$, where $k_m(t)$ is the value of k that maximizes S at a given t. Previous work has shown that, for many real systems and for three-dimensional computer models, the scaling function $F(x)$ depends only on the volume fraction ϕ of the minority phase but not on the temperature T for a given ϕ. Results from a Monte Carlo simulation of the two-dimensional Ising model, and also from a recently published numerical solution of the two-dimensional Cahn-Hilliard equation, are shown here to give a scaling function that can be fitted, as in the three-dimensional case, by an analytical expression containing just one adjustable parameter $\bar{\gamma}$, independent of T but dependent on ϕ. We analyze and interpret some universal features of these scaling functions, including their behavior at small x and at large x, and their dependence on ϕ. Our discussion is based on a two-phase model, i.e., a mixture of two types of domains separated by thin interfaces, with kinetics based on the Cahn-Hilliard equation. We introduce an assumption of self-similar evolution (in the sense of self-similar probability ensembles) and show that it leads to the well-known $t^{1/3}$ growth rate for the average domain size and to the above-mentioned universal properties of the scaling function. Simple geometric considerations also allow the calculation of the parameter $\bar{\gamma}$, so that the scaling function may be obtained without any adjustment of parameters. The influence of droplet-size distributions on the scaling function, the limit of very dilute alloys, and the temperature dependence of the coarsening rate are also considered.

I. INTRODUCTION

The kinetics of phase separation after quenching into the miscibility gap have been studied in a variety of two-phase systems ranging from liquid mixtures to solid alloys.[1-4] The dominant processes observed are the demixing of the homogeneous system into single phase regions and the subsequent increase in the average size of these regions, known as coarsening. The origin of this coarsening behavior is the tendency of the interfacial energy to decrease.[5,6] Other forces, such as elastic interactions in solids, may strongly alter the coarsening kinetics[7-9] and produce anisotropic cluster structures, for example, thin plates[10] but in this paper we consider only cases where the surface energy provides the only driving force for the coarsening.

In the late stages of this coarsening process the spherically averaged structure function $S(k,t)$, which can be measured experimentally using small-angle scattering of neutrons, x rays, or light,[1-3,11] has been found to satisfy a scaling relation. This scaling behavior was first observed in computer simulations[12] and appears to be a "universal" feature of the late stages of coarsening with (in three dimensions)

$$S(k,t)\sim k_m^{-3}(t)F(k/k_m(t)) ,$$

where F is a function of one variable and $k_m(t)$ is the value of k at which $S(k,t)$ has its maximum. It was further shown recently,[13] that for many different systems, including polymers, liquid mixtures, solid alloys, and theoretical models studied using computer simulations, the scaling function $F(x)$ can always be fitted by a formula that contains just one adjustable parameter, related to the volume fraction of the minority phase. That is, when the volume fraction is kept constant, $F(x)$ does not vary appreciably either with temperature or from one system to another. This "universality" of the structure function suggests that (for a given volume fraction) the spatial arrangement of the phases in the late stages of coarsening is also in some sense universal, systems as different as an acid-water mixture or an aluminum alloy having a similar

geometric arrangement of phases. This should be true at least over the ranges of distances corresponding to those where the structure function is measured and compared: for the acid-water mixture these distances would be of the order of micrometers and for the alloy of the order of nanometers.

Although there are various theoretical derivations of some properties of the shape of the scaling function $F(x)$, such as its small-x (Refs. 14 and 15) and large-x (Refs. 16 and 17) behavior, it is still far from clear what the essential features of the geometric arrangement of the phases leading to the universal shape of $F(x)$ are. What is clear from experiments[1–4,11] and computer simulations[18–21] is that the patterns at small volume fraction correspond to isolated droplets, whereas close to the critical mixture one observes interconnected spongelike structures. This description is, however, not precise enough to explain the universal character of the scaling function and its volume-fraction dependence. It is the aim of this paper to investigate, from both a theoretical and an empirical point of view, possible causes and implications of various apparently universal features of the scaled structure function. We give an outline of the contents of the paper at the end of the next section where we present definitions of the basic quantities.

II. DEFINITIONS

A. Structure function and scaling function

Consider any system of particles in which the ith particle scatters radiation with an amplitude u_i. For the binary mixtures we consider here, u_i takes one value u_A if the ith particle is an A particle and a different value u_B if it is a B particle. The scattering at any nonzero wavenumber shift $\mathbf{k}$ is proportional to the structure factor

$$S(\mathbf{k})=(1/N)\left\langle \left| \sum_{j=1}^{N} e^{i\mathbf{k}\cdot\mathbf{r}_j}(u_j-\bar{u}) \right|^2 \right\rangle , \tag{1}$$

where $\mathbf{r}_j$ is the position vector of the jth particle, N is the total number of particles in the system, and $\bar{u}$ is the average value of u_j,

$$\bar{u}=(1/N)\sum_{j=1}^{N} u_j . \tag{2}$$

The angular brackets signify an averaging over a suitable statistical ensemble; this averaging avoids mathematical difficulties when we take the Fourier transform to get the pair-correlation function. Of course the ensemble has to be chosen in such a way that the observed behavior of our macroscopic system is "typical" for the ensemble.[22]

For the phase-separating systems considered in this paper, it is found experimentally and in computer simulations that for large times t and a certain range of values of k the spherically averaged structure function at time t, which we denote by $S(k,t)$, takes a particularly simple "scaling" form, namely,

$$S(k,t)\simeq S(k_m(t),t)F(k/k_m(t)) \quad \text{for } 1/L \ll k \ll 1/\epsilon \text{ and large } t , \tag{3}$$

where $k_m(t)$ is (for each value of t) the value of k at which $S(k,t)$ takes its maximum value; L is the linear size of the system, and ϵ is some upper bound on the sizes of any microscopic structures in the system, such as lattice spacings, short-range interatomic correlations, and the thickness of the interfaces between phases. Most important of all, F is a function of one variable only, which we shall call the scaling function.

The pair correlation function $g(\mathbf{r})$ may be defined as the (inverse) Fourier transform of the structure function $S(\mathbf{k})$:

$$g(\mathbf{r})=(2\pi)^{-\nu}\int e^{-i\mathbf{k}\cdot\mathbf{r}}S(\mathbf{k})d^{\nu}\mathbf{k} \quad (r\neq 0) , \tag{4}$$

where the integral goes over all of ν-dimensional $\mathbf{k}$ space. A scaling relation may be written for the pair-correlation function in the form[19–21]

$$g(r,t)\simeq\bar{\bar{g}}(0,t)G(r/R_1(t)) \quad \text{for } \epsilon \ll r \ll L \text{ and large } t \tag{5}$$

where $g(r,t)$ denotes the spherical average of $G(\mathbf{r})$ at time t, $R_1(t)$ is the location of the first zero of $g(r,t)$ considered as a function of r, and $\bar{\bar{g}}(0,t)$ is to be understood as some limiting value of $g(r,t)$ when r is of order ϵ.

B. The two-phase model

Much of the theoretical discussion to be given in this paper will be based on the so-called two-phase model, already implicit in the work of Porod.[16] This model depends on the idea that at late times the system consists of two large regions Ω_A and Ω_B (neither of which need to be connected) whose local properties are similar to those of the equilibrium A-rich and B-rich phases, respectively, together with a thin interface region separating them. The thickness of the interface region, represented by a time-independent parameter ϵ, is much smaller than the length scale characterizing the sizes of the A-rich and B-rich regions. The two-phase model is an idealization arrived at by taking the limit $\epsilon\to 0$, that is, approximating the interface by a mathematical surface. At the same time, the system is also assumed to be infinite in extent, so that the finite-size effects disappear.

The structure function in the two-phase model, which we denote by $\tilde{S}$, is given by

$$\tilde{S}(\mathbf{k})=\lim_{|V|\to\infty}\left[|V|^{-1}\left\langle \left| \int_V [u_0(\mathbf{r})-\bar{u}]e^{i\mathbf{k}\cdot\mathbf{r}}d^{\nu}\mathbf{r} \right|^2 \right\rangle \right] , \tag{6}$$

where V is a region of space with some specified shape, say a sphere or a cube, $|V|$ is its volume, $u_0(\mathbf{r})$ is a function taking some specified constant value u_A if $\mathbf{r}$ is in Ω_A and a different value u_B if $\mathbf{r}$ is in Ω_B, and $\bar{u}$ is now the space average of $u_0(\mathbf{r})$:

$$\bar{u}=\lim_{|V|\to\infty}\left[|V|^{-1}\int_V u_0(\mathbf{r})d^{\nu}\mathbf{r}\right] . \tag{7}$$

Ideally, u_A and u_B should be chosen equal to the average scattering intensities per unit volume for bulk A-rich and B-rich phases. However, the structure functions $\tilde{S}$ obtained from different choices of u_A and u_B differ only by a constant factor and therefore give the same scaling

function F. For convenience we shall usually take $u_A=1$, $u_B=0$; then $\bar{u}$, as given by (7), becomes the volume fraction of phase A, which we denote by ϕ:

$$\bar{u}=\phi=\lim_{|V|\to\infty}(|\Omega_A|/|V|)\ , \tag{8}$$

where $|\Omega_A|$ denotes the volume of Ω_A.

The derivation of this model from the microscopic one in a suitable hydrodynamic limit $\epsilon\to 0$ and the proof of its validity as a good approximation in the late stages of coarsening is a central problem of the theory. Progress on this has been made recently by Pego[23] and others[24–26] starting from the Cahn-Hilliard equation.[27] This will be discussed in Sec. IV after we give in Sec. III an empirical fitting function for the $F(x)$, which incorporates all the experimentally (including computer simulation) observed features. We also discuss there the $t^{1/3}$ growth of $k_m^{-1}(t)$. All these properties can be derived, with varying degrees of conviction, from the statistical solutions of the Cahn-Hilliard or related equations, once we assume that the appropriate solutions are self-similar in time. The discussion of these points is the main content of Sec. V and the appendixes. Section VI contains some additional concluding remarks.

The derivation of Cahn-Hilliard-type equations from microscopic dynamics is currently an active area of research within the general context of the derivation of hydrodynamical equations from microscopic models. We shall not discuss these in this paper, but we refer the interested reader to Ref. 28.

III. THE SCALING FUNCTION IN TWO AND THREE DIMENSIONS

A. Construction of the model scaling function

In an earlier paper[13] we showed how to construct a model scaling function for the three-dimensional case. Here we extend these arguments to two dimensions.

We build up the model scaling function in three stages. The first stage is a two-phase model in which the interfaces are randomly placed lines in the plane. For the mathematical specification of this probability distribution, and of its three-dimensional analog, see Ref. 29. The two-point correlation function for this model is[30]

$$\tilde{g}(\mathbf{r})=\phi(1-\phi)e^{-\lambda r}\ , \tag{9}$$

where λ is a constant proportional to the amount of interface per unit area.

Next, to allow for the fact that the Fourier transform of $\tilde{g}$ has a maximum at some positive wave number k_m, so that $\tilde{g}$ itself is likely to have some kind of heavily damped oscillation, we multiply $\tilde{g}$ by an oscillating but decreasing function, to obtain

$$\tilde{g}(\mathbf{r})=\phi(1-\phi)\frac{\sin(2\pi r/\Delta)}{2\pi r/\Delta}e^{-\lambda r}\quad(\epsilon\ll r\ll L)\ , \tag{10}$$

where Δ is a "wavelength," which may be thought of as some kind of domain size.

It should be mentioned that the expression (10) is identical to the correlation function used by Teubner and Strey[31] to model the structure of microemulsions. Indeed, the structure of a dispersion of oil and water stabilized by surfactant molecules is qualitatively similar to the domain structure of a decomposing system. In the case of microemulsions, however, the structure corresponds to equilibrium and the correlation function (10) was obtained in Ref. 31 as the fluctuation spectrum for a phenomenological free energy.

The ν-dimensional Fourier transform of the right-hand side of (10) appears to give a good approximation to the experimental structure functions for wave vectors k near to or greater than k_m. However, for small values of k (corresponding to large distances) the scaled structure function should be proportional to k^4—this behavior will be discussed in more detail later (Sec. V A). As the third stage of constructing our model, therefore, we multiply the Fourier transform of the right-hand side of (10) by a factor $k^4/(k^4+\text{const})$, which is proportional to k^4 for small k and is close to 1 for large k.

Let us denote by $L_\nu(x)$ the approximate scaling function constructed in this way; in accordance with (3) it is calculated from the formula

$$L_\nu(x)=\tilde{S}(xk_m)/\tilde{S}(k_m)\ , \tag{11}$$

where k_m is the value of k that maximizes $\tilde{S}(k)$. The function L_ν has a simple analytical form for both $\nu=3$ (Ref. 13) and $\nu=2$ (Ref. 32):

$$L_\nu(x)=\frac{a_\nu x^4}{x^4+c_\nu}P_\nu(x)\ , \tag{12}$$

$$P_3(x)=\frac{b_3}{b_3+(x^2-1+d_3)^2} \tag{13}$$

and

$$P_2(x)=\frac{2}{\{(3+y^2)[y+(3+y^2)^{1/2}]\}^{1/2}}\quad\text{with } y=\frac{x^2-1}{b_2}-1+d_2\ , \tag{14}$$

and a_ν,b_ν,c_ν,d_ν are constants depending on λ and Δ. According to the definition (11) the maximum value of L_ν should be 1 and should occur when $x=1$. These two conditions fix a_ν and c_ν as functions of d_ν and b_ν. In three dimensions this argument gives[13]

$$c_3=\frac{d_3}{b_3-d_3(1-d_3)}\quad\text{and}\quad a_3=(1+c_3)\left[1+\frac{d_3^2}{b_3}\right] \tag{15}$$

while in the two-dimensional case it gives

$$\frac{c_2}{1+c_2}=\frac{[3+(1-d_2)^2]^{1/2}-2(1-d_2)}{4b_2[3+(1-d_2)^2]} \tag{16}$$

and

$$a_2=\frac{1+c_2}{2}([3+(1-d_2)^2]\{[3+(1-d_2)^2]^{1/2}-1+d_2\})^{1/2}\ . \tag{17}$$

The scaling function L_ν is thus characterized by two free parameters, b_ν and d_ν, which may be used for the fitting of experimental data. It should be noticed that for $d_\nu=0$ the x^4 correcting factor in L_ν disappears, because $c_\nu=0$ and $a_\nu=1$ in this case, and the remaining expression for the scaling function just corresponds to the Fourier transform of Eq. (10). The parameter d_ν is therefore a measure of the strength of the x^4 correction at small x.

B. Fitting of experimental scaling functions

Many three-dimensional data have been fitted in our previous paper.[13] It was found that the parameter d_3 could be given the value 0.06 in all the cases considered. A broad range of data are well described by this model scaling function,[13] and the agreement is much better than with earlier models.[2,33–35,25] It is therefore natural to fix d_3 to 0.06 in order to leave only one free parameter for the model scaling function.

In order to see whether a similar procedure is also possible in two dimensions we have performed Monte Carlo simulations of the Ising model on a 512×512 square lattice using the multispin updating algorithm of Amar, Sullivan, and Mountain.[36] For details of the implementation of this algorithm on a parallel computer, and a further description of the algorithm, see (Ref. 37). The algorithm is not mathematically equivalent to Kawasaki dynamics but is sufficiently similar that one may hope to obtain the same long-time behavior in the spherically averaged correlation and structure functions. Indeed, no irregularities appear in the correlation functions $g(\mathbf{r})$ or in the structure functions $S(\mathbf{k})$ at values of $\mathbf{r}$ or $\mathbf{k}$ corresponding to the period of the superlattice used in the multispin coding, which indicates that additional correlations introduced by the multispin coding are not very important.

Using the multispin algorithm, data were obtained up to 100 000 Monte Carlo steps (MCS), where the structure function is known from a previous study[36] to exhibit time-scaling behavior, and $S(k,t)$ was calculated by

TABLE I. Scaling parameters of the structure functions for the 2D Ising model.

ϕ	T/T_c	t (10^3 MCS)	$k_m(t)$	$S(k_m(t),t)$
0.5	0.8	20	0.19	5.6×10^{-4}
0.5	0.8	100	0.12	1.34×10^{-3}
0.5	0.5	4	0.44	1.1×10^{-4}
0.5	0.5	20	0.312	2.4×10^{-4}
0.5	0.5	100	0.20	5.8×10^{-4}
0.5	0.34	20	0.535	7.42×10^{-5}
0.5	0.34	100	0.405	1.4×10^{-4}
0.25	0.8	20	0.18	3.36×10^{-4}
0.25	0.8	100	0.117	8.5×10^{-4}
0.25	0.5	20	0.296	1.53×10^{-4}
0.25	0.5	100	0.197	3.5×10^{-4}
0.25	0.34	20	0.52	5.0×10^{-5}
0.25	0.34	100	0.385	9.0×10^{-5}
0.125	0.8	20	0.157	1.42×10^{-4}
0.125	0.8	100	0.105	3.45×10^{-4}
0.125	0.5	20	0.27	7.17×10^{-5}
0.125	0.5	100	0.178	1.65×10^{-4}
0.125	0.34	10	0.535	1.88×10^{-5}
0.125	0.34	20	0.481	2.28×10^{-5}
0.125	0.34	100	0.357	4.15×10^{-5}

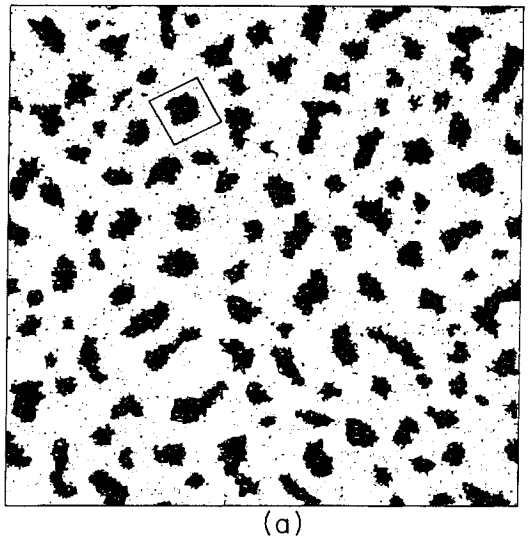

FIG. 1. Snapshot pictures of the two-dimensional Ising model (see Sec. III B) after 10^5 Monte-Carlo steps at the temperature $T=0.8T_c$ obtained using a multispin algorithm, which approximates Kawasaki dynamics. The volume fraction of the minority phase is in (a) $\phi=0.25$ and in (b) $\phi=0.5$. The square added onto each of the snapshot pictures has an edge length of $2\pi/k_m$, where k_m is the maximum position of the corresponding structure function $S(k)$ (see Table I).

averaging over typically 20–100 runs. Typical snapshot pictures of the two-dimensional Ising model at 100 000 MCS are shown in Fig. 1. Nine scaling functions were obtained at the temperatures $T/T_c = 0.34, 0.5, 0.8$ and the volume fractions $\phi = 0.125$, 0.25, and 0.5, by normalizing the structure functions according to Eq. (3). Some characteristics of these structure functions are shown in Table I. The scaling functions are shown in Figs. 2(a), 2(b), and 2(c). For each volume fraction ϕ, the data corresponding to different temperatures superpose, but for different volume fractions they are different. The results agree well with our finds[13] for the three-dimensional case. Some deviations from superposability are, however, to be seen in the region of very small x (Fig. 2), where the data show some scattering and do not even approach 0 when $x \to 0$. This may due to a finite-size effect, in the sense that the left-hand inequality of Eq. (3) is violated for the values of k corresponding to the smallest values of $x = k/k_m(t)$ plotted in the graph. In Figs. 2(a), 2(b), and 2(c) we also show the result of fitting the scaling functions in the range $0.2 \leq x \leq 4$ using the expression for L_2 [Eq.

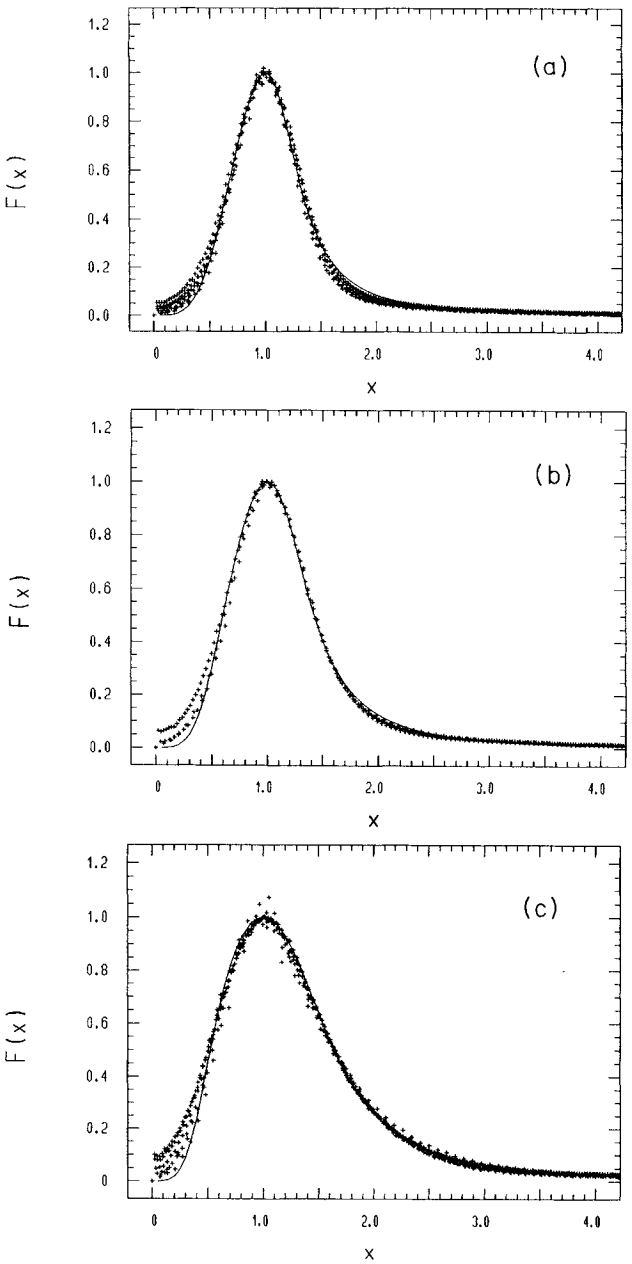

FIG. 2. Scaled structure functions of the two-dimensional Ising model for all temperatures, times, and volume fractions ϕ listed in Table I. The scaling functions for $\phi = 0.5$ are shown in (a), for $\phi = 0.25$ in (b) and for $\phi = 0.125$ in (c). The solid lines are fits to the data with Eqs. (12), (14), (16), and (17) and the values for the constants in these equations are given in Table II.

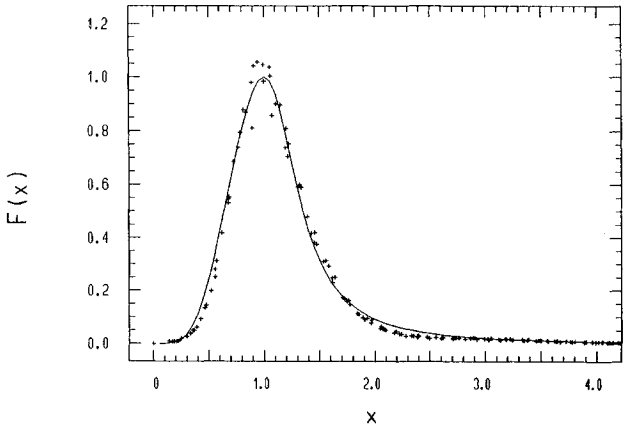

FIG. 3. Scaling function $F(x)$ for the solution of the Cahn-Hilliard equation from Ref. (19). The solid line is a fit to the data using Eqs. (12), (14), (16), and (17) with the values for the constants as given in Table II.

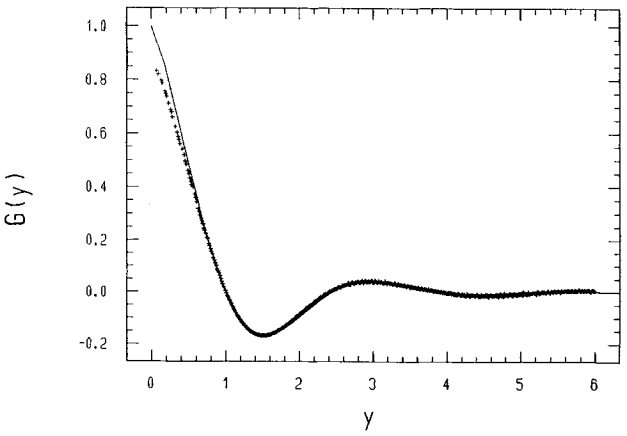

FIG. 4. Scaling function $G(y)$ for the solution of the Cahn-Hilliard equation from Ref. 20. The solid line is a fit to the data using the Fourier transform of Eqs. (12), (14), (16), and (17) with the values for the constants as given in Table II.

TABLE II. Summary of the parameters for the 2D model scaling functions.

	Ising model Present work			Cahn-Hilliard Equation Ref. 20	Ref. 19
ϕ	0.5	0.25	0.125	0.5	0.21
b_2	0.38	0.51	0.88	0.30	0.40
$\bar{\gamma}$	0.40	0.48	0.66	0.36	0.42

(12)] by a least-squares procedure. It turns out that the parameter d_2, characterizing the strength of the x^4 correction at small x, is not very critical for the fit and may be fixed at the value 0.60, leaving b_2 as the only free parameter. The values of this free parameter are given in Table II.

Numerical solutions of the two-dimensional Cahn-Hilliard equation have been published recently.[19–21] The data for $\phi=0.21$,[19] as well as for $\phi=0.5$,[20,21] were also fitted using L_2 and fixing $d_2=0.60$. The results may be seen in Figs. 3 and 4, where the Fourier transform of L_2 has been used to fit the scaled correlation function. The corresponding values of b_2 are listed in Table II. One will notice that the statistical variations of the data in the peak region (Fig. 3) are much stronger than in the case of the Ising model (Fig. 2). Nevertheless, the values of b_2 given by the Cahn-Hilliard equation are close to the corresponding values for the Ising model. From this analysis it seems, in contrast to earlier claims,[19] that the scaling function depends on volume fraction even for the Cahn-Hilliard model.

C. Dependence of k_m on time and temperature for the two-dimensional Ising model

As the scaling function for the two-dimensional Ising model at a given volume fraction is practically the same for all temperatures, it must be possible to absorb the whole temperature dependence of the decomposition process into the scaling parameter $k_m(t)$ listed in Table I. Surprisingly enough, one observes only a very small volume fraction dependence of $k_m(t)$ and a very simple temperature dependence: k_m depends on the time t and the temperature T only in the combination of $M(T)t$ where

$$M(T)=\frac{T_c}{T}e^{-8J/k_BT}, \tag{18}$$

where J is the Ising-model coupling constant and where we have taken $k_BT_c/J=2.2692$ for the two-dimensional Ising model.[36]

To illustrate this we give, in Fig. 5, a plot of the scaling length $2\pi/k_m$ against the quantity $[M(T)t]^{1/3}$. For each volume fraction ϕ the data points, regardless of temperature, lie close to a straight line. This shows that the dependence of k_m on t and T at fixed ϕ is approximately given by

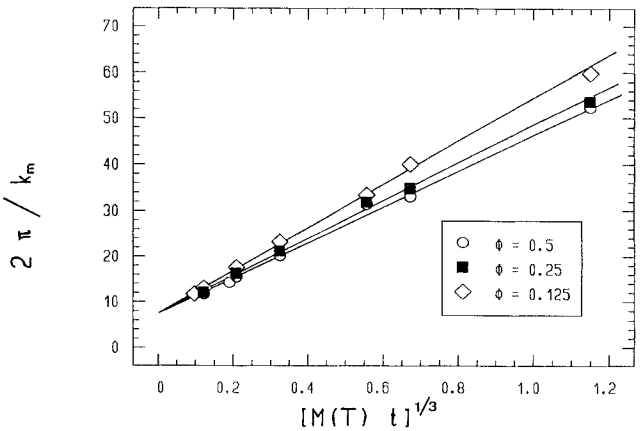

FIG. 5. Plot of $2\pi/k_m$, where k_m is the maximum position of the structure function for the Ising model (Table I), vs $[M(T)t]^{1/3}$, where t is the time measured in 10^3 MCS and $M(T)$ is given by Eq. (18). All data from Table I are included. The solid lines correspond to Eqs. (19) and (20).

$$\frac{2\pi}{k_m(t,T,\phi)}\approx A+B(\phi)[M(T)t]^{1/3}, \tag{19}$$

with

$$A\approx 8 \quad \text{and} \quad B\approx \begin{cases} 39 & \text{for } \phi=0.5 \\ 41 & \text{for } \phi=0.25 \\ 47 & \text{for } \phi=0.125 . \end{cases} \tag{20}$$

As far as the dependence on t at fixed T is concerned, these results agree with theoretical ideas due to Huse[38] and with earlier observations[36] of a time dependence proportional to $t^{1/3}+\text{const}$. For large T they also agree with the $t^{1/3}$ behavior of the domain size predicted by Lifshitz and Slyozov.[5] This $t^{1/3}$ behavior will be discussed further in Sec. IV C. The reason why the dependence on T has the particular form shown will be discussed in Sec. V D.

IV. THE TWO-PHASE MODEL: A MATHEMATICAL FRAMEWORK

A. Time evolution of the two-phase model

In this section we formulate a theory of the late stages of coarsening. We would like our theoretical picture to help us answer two questions: First of all, why does scaling work at all, and second, why does the scaling function depend on so few parameters?

Our discussion is based on the two-phase model, already described in Sec. II B. Space is divided into two regions Ω_A and Ω_B representing the two phases, separated by a mathematical surface, not necessarily connected, representing the interface. We shall call this surface Γ. The rule describing how the interface moves has been formulated by Mullins and Viñals[6] using a physical argument, and by Pego[23] using the Cahn-Hilliard equation.

Here we follow Pego's version. The Cahn-Hilliard equation is

$$\frac{\partial u}{\partial t}=c\nabla^2[f'(u)-\epsilon^2\nabla^2 u]\ , \tag{21}$$

where $f(u)$ is the equilibrium free-energy density when the order parameter is u. The function f has two local minima, and its convex envelope has a linear part on the interval $[u_A,u_B]$ but is otherwise strictly convex. The constant ϵ is proportional to the equilibrium thickness of an interface, and c is a rate constant, which is related to the interdiffusion constants D_A and D_B in the two phases A and B. The relationship, which can be obtained by linearizing (21) about $u=u_A$ and $u=u_B$, respectively, and setting $\epsilon=0$ [see Eq. (4.1) of Ref. 23], is

$$D_A=cf''(u_A),\quad D_B=cf''(u_B)\ . \tag{22}$$

To obtain the time-evolution rule for the interface, we consider the asymptotic behavior of the Cahn-Hilliard Eq. (21) in the limit of small ϵ and large t. This is done by rewriting (21) in the form

$$\epsilon\frac{\partial u^\epsilon}{\partial t_1}=\nabla^2\mu^\epsilon\ , \tag{23}$$

where μ^ϵ is defined by

$$\mu^\epsilon=f'(u^\epsilon)-\epsilon^2\nabla^2u^\epsilon \tag{24}$$

and t_1 by

$$t_1=c\epsilon t\ . \tag{25}$$

A formal asymptotic expansion in powers of ϵ indicates[23] that for small ϵ the solution $u^\epsilon(\mathbf{r},t_1)$ is close to its $\epsilon\to0$ limit $u_0(\mathbf{r},t_1)$ in most parts of space but that there are large deviations in certain layers of thickness $O(\epsilon)$ close to the interface. The existence of the $\epsilon\to0$ limit of $u^\epsilon(\mathbf{r},t_1)$ has not been proved rigorously, but in the corresponding problem for the related but simpler Cahn-Allen Eq. (39), written in the form

$$\epsilon^2\frac{\partial u^\epsilon}{\partial t_2}=\epsilon^2\nabla^2u^\epsilon-f'(u^\epsilon)\ , \tag{26}$$

where $t_2=\text{const}\times\epsilon^2t$, the existence of the corresponding limit has been proved, for suitable initial conditions, during the part of the motion where the surfaces remain smooth.[24]

The normal velocity v of the interface Γ (as measured on the t_1 time scale) is determined by the (nonlocal) law

$$v=[\mathbf{n}\cdot\nabla\mu_1]\ , \tag{27}$$

where $\epsilon\mu_1$ is the leading term in the ϵ expansion of the chemical potential, $\mathbf{n}\cdot\nabla\mu_1$ is the normal derivative of μ_1, and $[\mathbf{n}\cdot\nabla\mu_1]$ is the discontinuity in $\mathbf{n}\cdot\nabla\mu_1$ across Γ. The rule for determining μ_1 is

$$\begin{aligned}&\nabla^2\mu_1=0\ \text{ in }\Omega_A\text{ and }\Omega_B\ ,\\ &\mu_1=-\kappa\tau\ \text{ in }\Gamma\ ,\end{aligned} \tag{28}$$

where κ is the local mean curvature of Γ and τ is defined as

$$\tau=\int_{u_A}^{u_B}\sqrt{2[f(u)-(u-u_A)f'(u_A)]}\,du\ , \tag{29}$$

which in this theory is ϵ^{-1} times the surface tension.

To obtain the normal velocity on the physical t time scale, the value given in Eq. (27) should, because of (25), be multiplied by ϵc.

It could be argued that the Cahn-Hilliard equation is not a sufficiently accurate model of the phase separation process; for example, it does not include the phenomenon of diffusion along the interface, which according to Huse[38] is important at intermediate times. Nor does it include fluctuations, for which a stochastic model such as the Cahn-Hilliard-Cook equation[40] would be necessary. However, in the very late stages of phase separation, the Cahn-Hilliard equation does appear to be adequate, at least so far as determining the scaling function goes.

The Cahn-Hilliard equation is intended for the case of solid solutions, where the mechanism for the transport of the order parameter is diffusive and the thermal conductivity is high enough to keep the temperature constant. For other situations, for example in phase transitions involving fluids, the kinetic equations, and consequently the scaling behavior, may be different. However, one such case where we might still expect the same behavior is the demixing of a solution of two liquids of high thermal conductivity; in this case the combined Navier-Stokes and interdiffusion equations for the two components would be

$$\begin{aligned}&\frac{\partial\rho_A}{\partial t}+(\mathbf{w}\cdot\nabla)\rho_A=D_A\nabla^2(\mu_A-\mu_B)\ ,\\ &\frac{\partial\rho_B}{\partial t}+(\mathbf{w}\cdot\nabla)\rho_B=D_B\nabla^2(\mu_B-\mu_A)\ ,\\ &\frac{\partial\mathbf{w}}{\partial t}+(\mathbf{w}\cdot\nabla)\mathbf{w}=-\nabla p+\nu_K\nabla^2\mathbf{v}\ ,\end{aligned} \tag{30}$$

where ρ_A and ρ_B are the densities of the two components, μ_A and μ_B their local chemical potentials, $\mathbf{w}$ the fluid velocity, D_A and D_B are interdiffusion coefficients, p is the pressure and ν_K the kinematic viscosity. Provided that $D_A=D_B$ and p depends on ρ_A and ρ_B only in the combination $\rho_A+\rho_B$, these equations have solutions for which $\mathbf{w}$ is constant, while ρ_A and ρ_B vary in such a way that $\rho_A+\rho_B=\text{const}$ and

$$\frac{\partial(\rho_A-\rho_B)}{\partial t}=D\nabla^2(\mu_A-\mu_B) \tag{31}$$

so that we can apply arguments based on Eq. (21) to the order parameter $u=\rho_A-\rho_B$, while treating $\rho_A+\rho_B$ and $\mathbf{w}$ as constants.

B. Self-similar ensembles

Although the time evolution rule (27) is deterministic, our model is statistical because (in the mathematical model) the initial conditions are random. The actual surface configuration Γ at any positive time t can be thought of as drawn from a probability ensemble Π_t, analogous to the ensembles used in equilibrium statistical mechanics, though in the present case the analog of phase space is infinitely dimensional.

Just as in equilibrium statistical mechanics, there is no rigorous argument for choosing the right probability ensemble. In equilibrium statistical mechanics the standard hypothesis is based on the use, for sufficiently large times, of the simplest ensembles of all, that is, the ones in which the probabilities are independent of time. In the present case we shall adopt an analogous hypothesis and use, for large t, the simplest time-dependent ensembles, namely, the self-similar ones: that is to say, ensembles where the probabilities at any two different times are not identical but can be obtained from one another by spatial scaling. Some visual evidence in support of such an assumption can be obtained from pictures such as Fig. 1 of Ref. 20 in which typical configurations of interfaces for the two-dimensional Cahn-Hilliard equation for a given volume fraction at different times look very similar apart from a scale factor.

Unfortunately, in contrast to equilibrium statistical mechanics where the chosen ensemble is automatically consistent with the dynamics (being stationary with respect to the Hamiltonian flow), we have no proof at present that a self-similar ensemble actually exists, which is consistent with the asymptotic interface dynamics given by (21) and (28). We shall nevertheless assume that such an ensemble does exist and proceed to see what consequences follow.

To be precise, we shall say that a time-dependent ensemble Π of interface configurations Γ is self-similar if, given any two positive times t' and t'', one has a scaling factor $\beta(t,t'')$ such that

$$\Pi_{t''}(A)=\Pi_{t'}(\beta(t',t'')A) \tag{32}$$

for any set of configurations A having a definite probability. Here $\Pi_t(A)$ denotes the probability that at time t the interface configuration Γ belongs to the set A, and βA means the set obtained by dilating all the configurations in the set A by a factor β; that is,

$$\beta A=\{\beta\Gamma:\ \Gamma\in A\},\quad \text{where } \beta\Gamma=\{\beta\mathbf{r}:\ \mathbf{r}\in\Gamma\}\ . \tag{33}$$

The fundamental hypotheses of our mathematical model are these: (i) in the limit of large t the actual time-dependent probability ensemble approaches a self-similar one (we shall call this hypothesis *asymptotic self-similarity*) and (ii) the limiting self-similar ensemble is universal in the sense that (apart from trivial scale factors) it depends only on the conserved dynamical variables of the system—which, in the present case, means just the volume fraction.

The use of self-similarity as in ingredient in theoretical treatments of phase separation and coarsening has a long history—for references see Ref. 41. For example Mullins[41] (see also Ref. 6) uses a hypothesis that "consecutive configurations of the structure are geometrically similar in a statistical sense." What we believe to be new about the formulation given here is that our self-similarity hypothesis is applied to the time evolution of probability ensembles of interface configurations rather than that of individual interface configurations. The use of ensembles has the same advantages here as it has in other branches of statistical mechanics, namely, that the underlying probability assumptions can be formulated in a simple and precise way and the resulting theory developed in a way that ensures mathematical consistency without (for example) having to make special allowances for exceptional events of zero probability.

C. Some mathematical properties of self-similar ensembles

In this section we collect some mathematical consequences of the definition of self-similarity.

(i) For any self-similar ensemble, there is a function h such that

$$\beta(t',t'')=h(t')/h(t'')\ . \tag{34}$$

To prove this statement, let t',t'',t''' be any three positive times; then it follows from definition of β that

$$\beta(t',t''')=\beta(t',t'')\beta(t'',t''')\ . \tag{35}$$

Fix t''', define $h(t)=\beta(t,t''')$, and the proof is complete.

(ii) Let Φ be a length scale (defined below), and let the time-dependent ensemble Π be self-similar. Then $\Phi(\Pi_t)$ is proportional to $h(t)$.

By a length scale we mean a nonvanishing functional Φ of the probability distribution Π_t at time t, which is homogeneous of degree 1, i.e.,

$$\Phi(\alpha*\Pi_t)=\alpha\Phi(\Pi_t) \tag{36}$$

for all positive α, where $\alpha*\Pi_t$ denotes the dilated probability distribution defined by

$$\alpha*\Pi_t(\alpha A)=\Pi_t(A) \tag{37}$$

for all sets A, with αA defined as in (33). For example, $1/k_m$ is a length scale. To prove this result we note that the definition (32) of a self-similar ensemble can be written $\Pi_{t'}=\beta(t',t'')*\Pi_{t''}$. The definition (36) of length scale then gives

$$\Phi(\Pi_{t'})=\Phi(\beta(t',t'')*\Pi_{t''})=\beta(t',t'')\Phi(\Pi_{t''})\ .$$

Use the formula (34) for $\beta(t',t'')$, replace t' by t, and the result follows.

By similar methods we can prove that any functional, which is invariant under dilations, is independent of time: if $\Phi(\alpha*\Pi)=\Phi(\Pi)$ for all positive α, then $\Phi(\Pi_t)$ is independent of t. This property corresponds to one used by Mullins[41] (see also Ref. 6) as part of the description of his concept of statistical self-similarity.

(iii) For a self-similar ensemble of surface configurations the spherically averaged structure function defined as in (6) exactly satisfies a scaling relation analogous to (3):

$$\tilde{S}(k,t)=\tilde{S}(k_m(t),t)F(k/k_m(t))$$
$$\text{(for all } t \text{ and all } k>0)\ , \tag{38}$$

where $k_m(t)$ is the value of k (assumed unique for simplicity) that maximizes the left-hand side at fixed t. Moreover, $k_m(t)$ is proportional to $[h(t)]^{-1}$ and $S(k_m(t),t)$ is proportional to $[h(t)]^{\nu}$, where ν is the dimensionality.

Proof of (38). For any positive t',t'', the definition of self-similarity and the definition (6) of $\tilde{S}$ imply

$$\tilde{S}(k,t')=\beta^{\nu}\tilde{S}(\beta k,t'') , \tag{39}$$

where β means $\beta(t',t'')$. Combining with (34) we see that, given any positive number ξ, the expression $[h(t)]^{-\nu}\tilde{S}(\xi/h(t),t)$ has the same value, call it $\Psi(\xi)$, whether $t=t''$ or $t=t'$, and hence is the same for all positive values of t, so that we may write

$$\tilde{S}(k,t)=[h(t)]^{\nu}\Psi(h(t)k) .$$

Let ξ_m be the value of ξ that maximizes $\Psi(\xi)$; then we have from this last equation $k_m=\xi_m/h(t)$, proving one of the statements in the result (iii), and $\tilde{S}(k_m,t)=[h(t)]^{\nu}\Psi(\xi_m)$ proving another. Finally, defining $F(x)=\Psi(x\xi_m)/\Psi(\xi_m)$, we have

$$\frac{\tilde{S}(xk_m(t),t)}{\tilde{S}(k_m(t),t)}=F(x) , \tag{40}$$

which is equivalent to Eq. (38). In the case where the ensemble is only asymptotically self-similar, Eq. (40) will hold in the $t\to\infty$ limit:

$$\lim_{t\to\infty}\frac{\tilde{S}(xk_m(t),t)}{\tilde{S}(k_m(t),t)}=F(x) . \tag{41}$$

(iv) For a self-similar ensemble of surface configurations, which obeys the time-evolution rule (27) and for which the expectation of the interface area per unit volume (defined below) has a finite nonzero value, there is a constant t_0 such that

$$\beta(t',t'')=\left[\frac{t'-t_0}{t''-t_0}\right]^{1/3} \tag{42}$$

(after Mullins and Viñals[6]). By the interface area per unit volume we mean here

$$\sigma(\Gamma)=\lim_{|V|\to\infty}\left[|V|^{-1}\int_V dH(\Gamma)\right] , \tag{43}$$

where $dH(\Gamma)$ denotes the element of area on the interface surface Γ and V is as in (6).

The proof of Eq. (42) is given in Appendix A. To obtain the result (42) is not actually necessary to assume that the surface area per unit volume exists—any length scale will do instead—nor is it necessary to assume the particular time-evolution rule (27)—any rule which scales in the same way under space dilations will do—but the more general proof is longer. Equation (42) is equivalent to the statement that we may take the h in (34) to be

$$h(t)=(t+\text{const})^{1/3} . \tag{44}$$

(v) For an asymptotically self-similar ensemble of surface configurations obeying the time evolution rule (27), any length scale [for example $1/k_m(t)$] is asymptotically proportional to $t^{1/3}$. [Proof: use (44) in the result (ii).] The $t^{1/3}$ law was discovered by Lifshitz and Slyozov,[5] for the case of small volume fractions ϕ.

V. PROPERTIES OF THE SCALING FUNCTION AND THEIR INTERPRETATION

A. Small x behavior

1. The observations

Experimentally it is found[1-4] that $F(x)$ usually decreases to 0 when $x\to 0$ and, as pointed out recently by Yeung and Furukawa,[14,15] in many cases it is approximately proportional to x^4 in this limit. Small-angle scattering experiments and computer simulations are not always conclusive because there are natural limitations to the resolution which, in many cases, make it impossible to extend the measurements to very small x. Within these limitations, however, it has been found that many experimental data are indeed consistent with x^4 behavior at small x.[13] Assuming this x^4 law to be correct, it follows that not only

$$\lim_{x\to 0}F(x)=0, \quad \text{giving} \quad \lim_{k\to 0}\tilde{S}(\mathbf{k})=0 , \tag{45}$$

but also

$$\lim_{x\to 0}\frac{1}{x^{\nu-1}}\frac{\partial}{\partial x}\left[x^{\nu-1}\frac{\partial}{\partial x}\right]F(x)=0 ,$$

$$\text{giving} \quad \lim_{k\to 0}\nabla^2\tilde{S}(\mathbf{k})=0 . \tag{46}$$

2. Geometrical interpretation

To interpret these two equations, imagine a region V of given shape (e.g., the interior of a sphere) somewhere in the system, and define

$$M_0=\int_V[u(\mathbf{r})-\phi]d^{\nu}\mathbf{r} , \tag{47}$$

$$\mathbf{M}_1=\int_V[u(\mathbf{r})-\phi]\mathbf{r}\,d^{\nu}\mathbf{r} , \tag{48}$$

$$M_2=\int_V[u(\mathbf{r})-\phi]\mathbf{r}\cdot\mathbf{r}\,d^{\nu}\mathbf{r} . \tag{49}$$

Then it follows from (6), (45), and (46) that

$$\lim_{V\to\infty}\left[\frac{1}{|V|}\langle M_0^2\rangle\right]=\lim_{k\to 0}\tilde{S}(\mathbf{k})=0 , \tag{50}$$

$$\lim_{V\to\infty}\left[\frac{1}{|V|}\langle M_0M_2-\mathbf{M}_1^2\rangle\right]=-\tfrac{1}{2}\lim_{k\to 0}\nabla^2\tilde{S}(\mathbf{k})=0 . \tag{51}$$

Here $|V|$ denotes the volume of V.

The following simple morphological model may help to interpret these two equations. Suppose that the space occupied by the system can be divided into subregions V_j (we shall call them "boxes") which make independent random contributions $M_0^{(j)}$, $\mathbf{M}_1^{(j)}$, and $M_2^{(j)}$ to the integrals in (47), (48), and (49). Then, by taking the region V in (50) to be a union of subregions V_j and passing to the limit we find that (within this model) the expected value of $(\mathbf{M}_0^{(j)})^2$ is zero; that is, $M_0^{(j)}=0$ with almost complete certainty. Then, using this result in (51), we find that expected value of $(M_1^{(j)})^2$ is also zero, so that $\mathbf{M}_1^{(j)}=0$ almost certainly. In physical language, the frac-

tion of the A phase within every box is the same (we may call this condition "local conservation of matter"), and the centroid of the A phase within each box is at the centroid of the box.

In the case where the volume fraction is small enough for the minority phase to consist of isolated droplets or nuclei, each box comprises one nucleus together with the "depletion region"[42] surrounding it. The condition $M_0^{(j)}=0$ then has the physical interpretation that, on average, all the superfluous B atoms in the depletion region within V_j have been eaten up by the nucleus at its center, rather than escaping into other boxes. The condition $\mathbf{M}_1^{(j)}=0$ then has the interpretation that the nucleus is at the centroid of V_j rather than being at its edge: as it grows, the nucleus draws in matter even handedly from all sides.

To make these ideas more quantitative, let us consider a one-dimensional example. In this case the two-phase model consists of alternating segments of the two phases, the lengths of the segments being chosen according to some probabilistic rule. These segments correspond to the boxes defined above. The simplest case to consider would be one where the lengths of the different intervals are independent [Fig. 6 (i)]. However, as we have just seen, such a model cannot give the right behavior for small x: because the condition $M_0^{(j)}=0$ is not satisfied, $\tilde{S}(0)$ is bound to have a positive value. For example, if the lengths have a Poisson distribution, then $g(r)$ is exponential and $\tilde{S}(k)$ is a Lorentzian. In general, the explicit calculation shows [see Appendix C 1] that for independent intervals $\tilde{S}(0)$ always has a positive value, violating the condition (45).

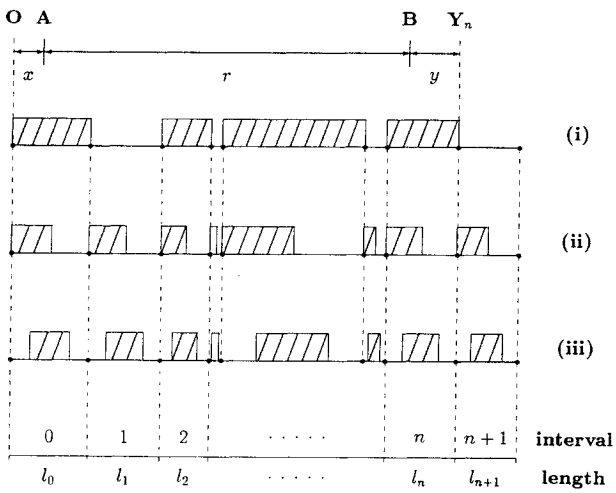

FIG. 6. One-dimensional two-phase models. l_n is the length of the nth interval on the line. The shaded areas are the regions occupied by the black phase and the rest is occupied by white phase. In model (i) the intervals are colored alternately black or white. In model (ii) the left part of each interval is black, and in model (iii) the center part of each interval is black.

The condition of local conservation of matter may be introduced into the linear model by requiring each $M_0^{(j)}=0$ [see Appendix C 2]. In Fig. 6 (ii) the left part of each box is colored black and the rest is white. The corresponding scaling function is calculated in Appendix C2. Now the global shape of the scaling function is already obtained, but because the centroid condition is still violated the function is proportional to x^2 rather than x^4 at small x.

The introduction of the centroid condition $\mathbf{M}_1=0$ into the linear model is achieved by simply shifting the black phase into the center of each interval (Fig. 6) The corresponding scaling function then has, indeed, the right x^4 behavior at small x (Appendix C 3).

3. *Theoretical explanation of the x^4 law*

The observation that $F(x)$ is proportional to x^4 at small x can be understood qualitatively from the following argument, due in essence to Yeung[14] and Furukawa.[15] Let $u_{\mathbf{k}}$ and $\mu_{\mathbf{k}}$ be the Fourier transforms of u and μ, respectively. Then the Cahn-Hilliard equation (21) implies

$$\frac{\partial u_{\mathbf{k}}}{\partial t}=-k^2 c\mu_{\mathbf{k}}(t)\ . \tag{52}$$

This suggests that $u_{\mathbf{k}}$ is likely to be proportional to k^2 at large times and hence that $\tilde{S}(\mathbf{k},t)$, which is the expectation of $|u_{\mathbf{k}}|^2$, is likely to be proportional to k^4 at fixed t. From this behavior of $\tilde{S}$ the x^4 behavior of $F(x)$ would follow.

However, to make the argument work, we need to know something about the behavior of $\mu_{\mathbf{k}}(t)$ for small k and large t. Yeung[14] assumes, in effect, that $\mu_{\mathbf{k}}(t)$ times a certain function of t is bound as $k\to 0$ for all t, but he does not give the justification for this assumption. Furukawa's derivation[15] also depends on an assumption, multitime scaling, some evidence for which is given in Ref. 43. A derivation of the x^4 law, which does not require any fresh assumptions, is given in Appendix B.

B. Large x-behavior

1. *Porod's law*

The theory of the behavior of $\tilde{S}(k)$ for large k is due to Porod.[16,17] He showed that the two-point correlation function of the two-phase model (with $u_A=1$, $u_B=0$) behaves for small r according to

$$\tilde{g}(r,t)=\phi(1-\phi)-K_\nu\sigma(t)r+o(r)\quad\text{as } r\to 0\ , \tag{53}$$

where K_ν is a constant depending on the number of dimensions ($K_2=1/\pi$, $K_3=\frac{1}{4}$), $\sigma(t)$ is the area of interface per unit volume, and $o(r)$ denotes a quantity (for example r^2), which goes to 0 more rapidly than r as $r\to 0$. By using the Fourier transform relation (4), Eq. (53) can be shown[17,42] to imply [provided that $g(r)$ is twice differentiable for $r\neq 0$] that

$$\tilde{S}(k,t)\sim K'_\nu\sigma(t)k^{-\nu-1}\quad\text{as } k\to\infty\ , \tag{54}$$

where $K'_2=2$ and $K'_3=2\pi$. Comparing the definitions (4)

and (53) for $r=0$, it follows for $\nu=2$ or 3,[44]

$$\int_0^\infty k^{\nu-1}\tilde{S}(k,t)dk=\pi\phi(1-\phi)K'_\nu$$
$$=\frac{\pi\phi(1-\phi)}{\sigma(t)}\lim_{k\to\infty}k^{\nu+1}\tilde{S}(k,t)\ . \qquad (55)$$

This implies, by (38), that $F(x)\sim\text{const}\times x^{-\nu-1}$ for large x, with a constant of proportionality, which does *not* depend on t.

To observe Porod's law (54) in a real system we must look at distances that are large compared with the thickness ϵ of an interface but small compared with the sizes of the domains. A typical domain size is of order $1/k_m$, so that the condition for $k^{-(\nu+1)}$ decay is $k_m \ll k \ll 1/\epsilon$. In the late stages of phase separation, the domain size is much bigger than the thickness of the interfaces, so that $k_m \ll 1/\epsilon$, and there is a range of k values in which Porod's law can hold.

Experimentally it is not always possible to determine the behavior of $S(k)$ at large k with high accuracy because the small scattering intensities at large wave numbers lead to difficulties with background subtraction and counting statistics. However, where this behavior has been determined, it has generally been found to agree with Porod's law $S(k)\propto k^{-(\nu+1)}$.

2. Size distribution of the monophase domains

Porod's law gives the leading term for the decrease of $S(k,t)$ at large k values, but in principle there could be oscillations around this leading term. Such oscillations would, for instance, be observed[17,42,44] for a monodisperse distribution of spheres or other regular objects (such as cubes, ellipsoids, etc.). In practice, such oscillations are not usually observed (an exception will be discussed in Sec. IV D 3) and in the model scaling function considered in Sec. III they do not appear. This absence of oscillations for the model scaling function is mainly due to the exponential damping factor in Eq. (10), which corresponds to the fact that the sizes of the monophase domains vary strongly along any line through the sample. This also means that the size distribution of the monophase domains must be significantly broader than the one derived by Lifshitz and Slyozov[5] (see Sec. IV D 3).

It is not easy to make general quantitative predictions about the size distribution, just from the shape of the scaling function without additional assumptions. Some qualitative impressions may, however, be gained by use of the linear model introduced in Sec. V A 2 and illustrated in Fig. 6 (iii). The model consists of a succession of intervals on a line, with lengths that are independently chosen at random from some given probability distribution p. Each interval (with length l, say) contains in its center a region of A-rich phase of length ϕl with regions of B-rich phase on either side, so that the corresponding scaling function has the right behavior at small and large x. Using a distribution for l of the type

$$p_n(l)=\frac{n\rho}{\Gamma(n)}(n\rho l)^{n-1}e^{-n\rho l}\ , \qquad (56)$$

we can vary the width of the size distribution by changing the value of n. For various values of n, the distribution of l and the corresponding scaled structure function (for $\phi=0.5$) are shown in Figs. 7(a) and 7(b), respectively. It can be clearly seen that a secondary maximum starts to appear as soon as the width of the distribution is smaller than the average size ρ^{-1} of the intervals. Assuming that some analog of this result applies in higher dimensions, the conclusion would be that the width of the distribution of domain sizes should be about as large as the average size itself in order to avoid oscillations around the dominant decay of $F(x)$ at large x. In case the size distribution is somewhat narrower, i.e., if there is more periodicity in the spatial structure than expected from the model outlined in Eq. (10), a bump may appear in the region of larger x [see the curve for $n=5$ in Fig. 7(b)] giving a possible explanation for the occurrence of such a bump reported recently in the case of a polymer mixture[45] and for recent numerical results using a cell-dynamical system.[46]

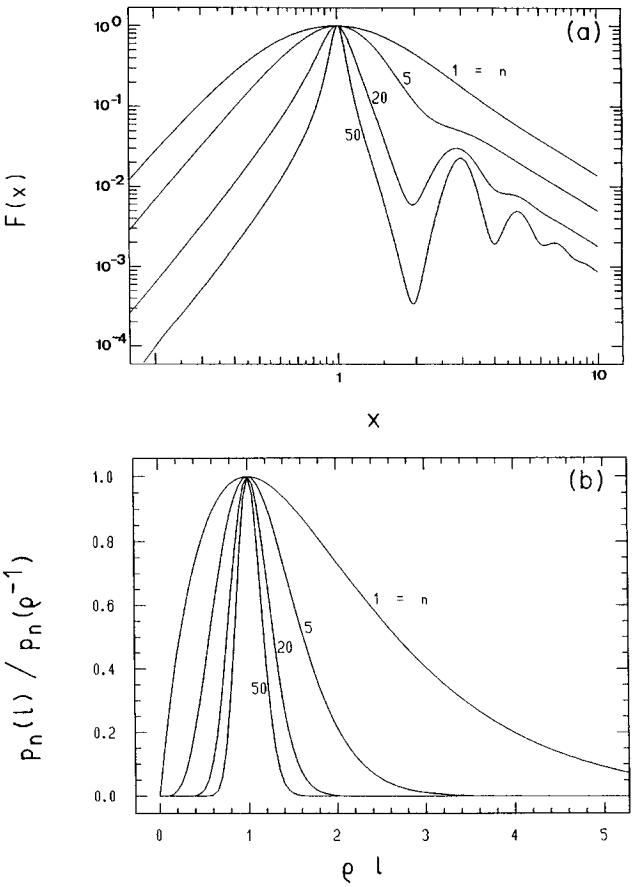

FIG. 7. Illustration of oscillations of the scaling function $F(x)$ [shown in (a)] around the average decrease at large x (given by Porod's law), when the width of the size distribution [shown in (b)] of the monophase domains is changed. The figure shows the data for the one-dimensional model (iii) of Fig. 6 with $\phi=0.5$ and where the size distribution of the interval length l_j is given by Eq. (56). n is the parameter appearing in Eq. (56).

C. Dependence of the peak width on volume fraction

1. The observations

From the fits of experimentally determined scaling functions in three[13] and two dimensions (Sec. III) it has become apparent that there is a well-defined dependence of $F(x)$ on the volume fraction ϕ but that, for a given ϕ, the scaling function is essentially independent of temperature. The main dependence on volume fraction is an increase of the peak width when ϕ is decreased. Similar conclusions were also reached from investigations of aluminum alloys with different compositions.[34,11]

2. Theoretical interpretation

As a measure of the width of the graph of $F(x)$, we introduce a quantity $\tilde{\gamma}$ defined by

$$\tilde{\gamma} \equiv \frac{\lim_{x\to\infty}[x^{\nu+1}F(x)]}{\int_0^\infty x^{\nu-1}F(x)dx} . \tag{57}$$

A small value of $\tilde{\gamma}$ corresponds to a narrow peak; for example if F is a δ function, then $\tilde{\gamma}$ is zero. Using (57), the value of $\tilde{\gamma}$ can be calculated for any of the model scaling functions L_ν developed in Sec. III; some examples are shown in Table II. In this way $\tilde{\gamma}$ can be expressed as a function of the parameter b_ν characterizing the function L_ν.

Using ideas already introduced in Ref. 13, we can calculate $\tilde{\gamma}$ theoretically, once ϕ is known, and hence deduce b_ν and the entire scaling function via the relationship between $\tilde{\gamma}$ and b_ν just mentioned. The key is the relation (55), which when combined with (57) gives

$$\tilde{\gamma} = \frac{\sigma(t)k_m^{-1}(t)}{\pi\phi(1-\phi)} , \tag{58}$$

where $\sigma(t)$ is the amount of surface area per unit volume. To use this formula we need values for $k_m(t)$ and $\sigma(t)$. We estimate $k_m(t)$ as

$$k_m(t) \approx 2\pi/\Delta(t) , \tag{59}$$

where $\Delta(t)$ is the average linear dimension of the boxes V_j introduced in Sec. IV B 2. [This identification would be exact if the boxes were all identical, forming a lattice with period $\Delta(t)$.] To calculate $\sigma(t)$ we need an assumption about the shape of the interface. At low volume fractions the minority phase is assumed to consist of spherical droplets, one to each box [see Fig. 1(a), where a box of size $2\pi/k_m$ is drawn on a typical snapshot picture for the two-dimensional Ising model at $\phi=0.25$]. It should be mentioned that, in the Ising model, the droplets are not completely spherical due to the anisotropy of the surface tension [Fig. 1(a)]. This weak nonuniversality is, however, washed out in the spherically averaged structure factors considered here. The average radius $R(t)$ of the (spherical) droplets is related to ϕ by

TABLE III. Calculation of $\tilde{\gamma}=k_m^{-1}\sigma/\pi\phi(1-\phi)$. σ is the interphase surface per unit volume. ϕ is the volume fraction of the minority phase.

	Dimension 3	Dimension 2
k_m	$2\pi/\Delta$	$2\pi/\Delta$
Morphology	Sphere of radius R	Disk of radius R
$\sigma\Delta$	$4\pi\left[\frac{R}{\Delta}\right]^2$	$2\pi\frac{R}{\Delta}$
ϕ	$\frac{4}{3}\pi\left[\frac{R}{\Delta}\right]^3$	$\pi\left[\frac{R}{\Delta}\right]^2$
$\tilde{\gamma}$	$\left[\left[\frac{2\pi^5}{9}\right]^{1/3}\phi^{1/3}(1-\phi)\right]^{-1}$	$[\pi^{3/2}\phi^{1/2}(1-\phi)]^{-1}$
Morphology	Cylinder of radius R	Stripe of thickness $2R$
$\sigma\Delta$	$2\pi\frac{R}{\Delta}$	2
ϕ	$\pi\left[\frac{R}{\Delta}\right]^2$	$2\frac{R}{\Delta}$
$\tilde{\gamma}$	$[\pi^{3/2}\phi^{1/2}(1-\phi)]^{-1}$	$[\pi^2\phi(1-\phi)]^{-1}$
Morphology	Plate of thickness $2R$	
$\sigma\Delta$	2	
ϕ	$2\frac{R}{\Delta}$	
$\tilde{\gamma}$	$[\pi^2\phi(1-\phi)]^{-1}$	

$$\text{const}\times[R(t)]^{\nu}=\phi[\Delta(t)]^{\nu} \tag{60}$$

and to $\sigma(t)$ by

$$\text{const}\times[R(t)]^{\nu-1}=\sigma(t)[\Delta(t)]^{\nu}\ , \tag{61}$$

so that, eliminating $R(t)$, we obtain $\sigma(t)\approx\text{const}\times\phi^{1-1/\nu}/\Delta(t)$. Thus by substitution into (58), using (59), our theoretical formula for $\bar{\gamma}$ at low densities takes the form

$$\bar{\gamma}\approx\text{const}\times\phi^{-1/\nu}(1-\phi)^{-1}\ . \tag{62}$$

For the value of the constant see Table III.

At higher volume fractions this droplet picture is no longer correct, and the regions occupied by the two phases become interconnected. A rough representation of the interconnected patterns may be obtained by assuming that in each box of size $\Delta(t)$ there is now a cylinder, or in two dimensions a stripe, crossing the box. A typical box is shown in Fig. 1(b), a typical snapshot picture of the configuration of the two-dimensional (2D) Ising model at $\phi=0.5$. As the stripes (or cylinders) in adjacent boxes may have different orientations, this would describe a highly interconnected structure. For three dimensions one may also imagine an arrangement consisting of interconnected plates rather than cylinders. The relevant calculations are summarized in Table III.

It is interesting to note that the total interface surface for a given volume of the B phase inside the box is, in three dimensions,[13] smaller for the cylinder than for the droplet if the value of ϕ is larger than about 0.15, and even smaller for the plate if $\phi>0.31$ (taking $\phi\leq 0.5$ throughout). In two dimensions the surface area of the stripe is smaller than that of the droplet for $\phi>0.31$ (see Table III). The calculation thus provides a rough quantitative explanation of why nature favors an interconnected structure rather than isolated droplets at the higher volume fractions.

3. *The case of infinite dilution*

In the infinite dilution limit, the droplets will be spherical because of surface tension and their separation will become extremely large. Consequently, there will no longer be any interference between droplets and the structure function will have its maximum at (or at least very close to) $k=0$.[17] This fact is in contradiction to experimental data for systems with finite ϕ,[3,13] but seems to be supported by some recent experiments with extremely dilute systems.[47] According to the model outlined in Sec. III and Table III the width of the graph of $F(x)$ diverges as $\phi\to 0$, which also indicates that the maximum of the structure function should be located at $k=0$ in the limit when $\phi=0$.

An explicit expression for the size distribution of the monophase domains in the limit $\phi\to 0$ is given by the theory of Lifshitz and Slyozov (LS).[5] Using this expression, the limiting structure function can be calculated explicitly, and we give the result here.

For $\phi\to 0$, the probability $P(R)dR$ that a droplet has a radius between R and $R+dR$, is calculated by LS (Ref. 5) as

$$P(R)=p(R/\bar{R}(t))/\bar{R}(t)\ , \tag{63}$$

where $\bar{R}(t)$ is the time-dependent average radius and

$$p(x)=\begin{cases} 3^4 2^{-5/3}x^2(x+3)^{-7/3}(\frac{3}{2}-x)^{-11/3}e^{1-[1-(2/3)x]^{-1}} & \text{for } x\leq\frac{3}{2} \\ 0 \quad \text{for } x\geq\frac{3}{2}\ . \end{cases} \tag{64}$$

Assuming spherical droplets with this size distribution and no interference between these droplets (i.e., $\phi\to 0$), the corresponding structure function $S(k,t)$ can be computed using the Rayleigh function Ξ^2:[17]

$$S(k,t)=S(0,t)\frac{\int_0^{\infty}R^6\Xi^2(kR)P(R)dR}{\int_0^{\infty}R^6P(R)dR}\ , \tag{65}$$

where

$$\Xi(x)=3\frac{\sin x-x\cos x}{x^3}\ . \tag{66}$$

A scaling function according to Eq. (3) cannot be defined in this case because $k_m=0$, but one may define in analogy the function F_{LS} by

$$F_{\text{LS}}(x)=\frac{S(x\bar{R}^{-1}(t),t)}{S(0,t)}=\frac{\int_0^{\infty}u^6\Xi^2(xu)p(u)du}{\int_0^{\infty}u^6p(u)du}\ . \tag{67}$$

F_{LS} is plotted in Fig. 8 together with the Rayleigh function Ξ^2 corresponding to a monodisperse system of spherical droplets.

Several properties of F_{LS} appear on this graph. First, the maximum of F_{LS} is located at $x=0$, as already mentioned. Then, there are some shoulders appearing at large x, which are the remains of the maxima of the Rayleigh function, slightly smoothed by the averaging over $P(R)$. In fact, these shoulders correspond to oscillations around the average decrease x^{-4} (Porod's law). Finally, it is easy to imagine that on averaging the Rayleigh function using broader size distributions than the one predicted by LS (Ref. 5) the oscillations will disappear complete-

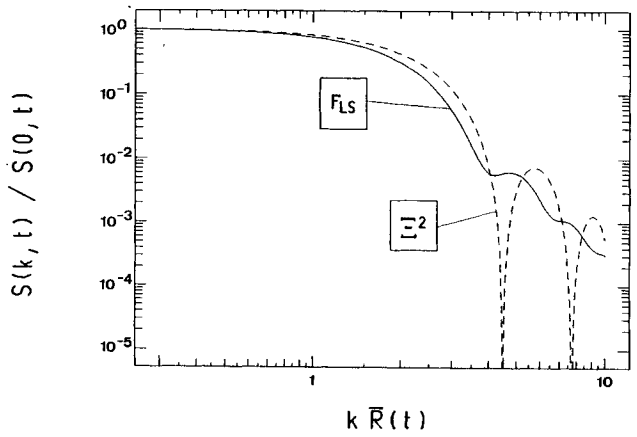

FIG. 8. Scaled structure function for isolated spherical droplets (dashed line) and after averaging with the size distribution predicted by Lifshitz and Slyozov for very dilute systems (Ref. 5) (solid line). The solid line corresponds to $F_{LS}(x)$ as given by Eq. (67) and the dashed line to $\Xi^2(x)$ as given by Eq. (66).

ly, leaving only the x^{-4} decay. Indeed, all extensions of the original LS theory to finite (but still small) volume fractions ϕ (Ref. 48) predict broader distribution functions than LS. This might explain why oscillations around the x^{-4} decay (Porod's law) are usually not found in experiments where ϕ is finite.[3,13] Recent data on very low-density systems ($\phi<0.01$), indeed, suggest the disappearance of the interference maximum in the structure function when $\phi\to 0$ and give experimental evidence for oscillations around the x^{-4} decrease.[47]

D. Dependence of length scale on temperature for the Ising model

In Sec. III C we noted that for the two-dimensional Ising model k_m depended on T and t only in the combination $M(T)t$, with $M(T)$ given by (18). Here we show how this result can be understood as a consequence of the theory developed in this section, particularly Sec. V D 4. There we saw [Eq. (25)] that the time scale appropriate for describing the motion of the interfaces in the two-phase model was

$$t_1 = c\epsilon t \ . \tag{68}$$

Imagine two systems started with the same probability ensemble (and hence the same value of the volume fraction ϕ) and then allowed to evolve at different temperatures. By the time that t_1 has reached a value, which is $O(1)$ [so that $t=O(1/\epsilon)$], Eq. (27) is predicting that on the t_1 time scale the velocities of a given surface Γ in the two ensembles are in proportion to the values of τ [defined by Eq. (29)]. If we used instead τt_1 as our time variable then the surface would have identical velocities in the two ensembles. Thus the theory predicts that, for a given ϕ, the value of k_m depends on T and t_1 only in the combination τt_1, which, by (25), is related to the physical time t by

$$\tau t_1 = \tau c\epsilon t \ . \tag{69}$$

For the Ising model at temperatures low enough for the minority phase to be effectively an ideal lattice gas, we can calculate c explicitly. In this calculation we depart from our usual convention of taking $u_A=1$, $u_B=0$. Taking u instead to be the concentration of A atoms in a B-rich phase, we can write the free energy of the system approximately as

$$F=E-TS\simeq Nu\ \delta E-k_BT\ln\left[\frac{N!}{(Nu)![N(1-u)]!}\right], \tag{70}$$

where E is the energy, S the entropy, k_B Boltzmann's constant, N the number of lattice sites, and δE the energy increase on replacing one A atom by a B atom when all the neighboring atoms are A. The free energy per site is therefore

$$f(u)\simeq u\ \delta E+k_BT[u\ \ln u+(1-u)\ln(1-u)] \ . \tag{71}$$

Hence, by (22), the interdiffusion coefficient is

$$D_A\simeq ck_BT/u \ . \tag{72}$$

Since we also have, at low temperatures,

$$u=e^{-\delta E/k_BT}, \tag{73}$$

it follows that

$$\begin{aligned} c&=(D_A/kT)e^{-\delta E/k_BT}\\ &=(D_A/k_BT)e^{-8J/k_BT} \end{aligned} \tag{74}$$

for the two-dimensional Ising model. Thus the right combination of t and T at low temperatures is, by (69),

$$\tau t_1=(\tau\epsilon D_A/kT)e^{-8J/k_BT}t \ . \tag{75}$$

This is of the form used in Sec. III C, with

$$M(T)=\text{const}\times(\tau\epsilon D_A/kT)e^{-8J/k_BT} \ . \tag{76}$$

For Kawasaki dynamics using (for example) the Metropolis probability rule the interdiffusion coefficient D_A is independent of temperature at low temperatures, and the surface tension $\tau\epsilon$ will vary with temperature much more slowly than the exponential factor; so we expect the simple formula for $M(T)$ given in (18) to give good results provided the temperature is not too high.

Although the derivation given above is based on the Cahn-Hilliard equation, the result does not stand or fall by that equation, since it really depends only on the interface evolution law (27). The essential point is that the velocity of a given interface is proportional to the product of three factors: (a) the ratio (surface tension)/kT, which determines the excess density of minority atoms near a surface of given curvature, (b) the equilibrium density of minority atoms, and (c) the interdiffusion coefficient.

VI. CONCLUSION

Some apparently universal features of the scaling function for liquid or solid systems (with negligible coherency stresses) undergoing phase separation were analyzed, and the following conclusions were reached.

(a) For the two-dimensional Ising model, we see evidence that the scaling function depends on the volume fraction ϕ but not on the temperature. This confirms an earlier investigation of three-dimensional systems (real systems as well as computer simulations).[13]

(b) The 2D scaling function for the Ising model and for the solution of the Cahn-Hilliard equation can be fitted, as in the three-dimensional case,[13] by a simple analytic expression containing just one adjustable parameter related to the volume fraction ϕ.

(c) The temperature dependence of the decomposition process in the late stages of coarsening is found to be absorbed into the temperature dependence of the scaling length $2\pi/k_m$ as a function of time. For the case of the 2D Ising model with Kawasaki dynamics, $1/k_m(t)$ is only slightly dependent on ϕ, and its temperature dependence is mainly due to the temperature dependence of the density of minority atoms in a thermodynamically pure phase.

(d) A theoretical interpretation of some features of the scaling function $F(x)$ was given, based on Pego's asymptotic analysis of the Cahn-Hilliard equation and on the hypothesis of asymptotic self-similarity. This includes the following.

(i) The universal character of F: the fact that F is determined by just one parameter, the volume fraction, is interpreted as a consequence of the hypothesis that the asymptotically self-similar ensemble of interface configurations is completely determined by the one invariant of their time evolution—the volume fraction.

(ii) The large-x behavior of $F(x)$: Porod's law [$F(x)\sim x^{-4}$ as $x\to\infty$] is observed because in the late stages of coarsening the typical domain size becomes much larger than the thickness of the interfaces.

(iii) The small-x behavior of $F(x)$: a dependence $F(x)\sim x^4$ as $x\to 0$ follows from the hypothesis that domain growth is governed by the Cahn-Hilliard equation. For the morphology of the two-phase system this implies a local conservation of the order parameter as well as a kind of "local symmetry."

(iv) The ϕ dependence of $F(x)$: a broadening of the maximum in the graph of $F(x)$ versus x is found when ϕ decreases. With the approximation that the conservation of order parameter holds exactly within boxes of a size (several times) $2\pi/k_m(t)$, k_m being the maximum of the structure function, it is possible to predict the only free parameter in the analytical expression for the scaling function, and hence the ϕ dependence of the width of the scaling function.

Taken together, these points give some explanation for the universal character of the scaling function and, knowing the phase diagram, allow the prediction of a model scaling function, without any adjustable parameter, which can be directly compared with experiment.

ACKNOWLEDGMENTS

We are grateful to J. Carr, R. L. Pego, and B. Tóth for helpful discussions, to R. Toral and R. Desai for sending us their numerical data on the solution of the Cahn-Hilliard equation, to the National Science Foundation (NSF) under Grant No. DMR-89-18903, the Science and Engineering Research Council (SERC), and the British Council for financial support, and to the Institut des Hautes Etudes Scientifiques, Bures-sur-Yvette, France, for its hospitality during a visit where part of this work was done.

APPENDIX A: PROOF OF EQ. (42)

Lemma. Let $X(\Gamma)$ be a function of the interface configuration, which is homogeneous of degree n for some nonzero integer n, i.e., $X(\alpha\Gamma)=\alpha^n X(\Gamma)$. Then $\langle X\rangle^{1/n}$ is a length scale and $\langle X\rangle$ is proportional to $[h(t)]^n$.

Proof of lemma. The value of the functional in the ensemble $\alpha * \Pi$ is, by definition,

$$\begin{aligned}\langle X\rangle_{\alpha*\Pi} &= \int X(\Gamma)d(\alpha*\Pi(\Gamma)) \\ &= \int X(\Gamma)d(\Pi(\alpha^{-1}\gamma)) \quad \text{by (36)} \\ &= \int X(\alpha\Gamma')d(\Pi\gamma') \quad \text{defining } \Gamma=\alpha\Gamma' \\ &= \alpha^n \int X(\Gamma')d(\Pi\gamma') \,, \\ &\qquad\qquad \text{since } X(\Gamma) \text{ is homogeneous} \\ &= \alpha^n\langle X\rangle_\Pi \quad \text{by definition} \,. \end{aligned} \tag{A1}$$

This proves the first part of the lemma, and the second part then follows at once from the theorem (ii) in Sec. IV C.

Proof of Eq. (42). Consider the surface area per unit volume σ, defined in (43). Its time rate of change is, in terms of the normal velocity v of the interface and its local mean curvature κ,

$$\frac{d}{dt}\sigma(\Gamma(t)) = \lim_{|V|\to\infty}\left[\int_V v\kappa\, dH(\Gamma(t))\right] , \tag{A2}$$

since the contributions to $(d/dt)\int_V dH(\Gamma)$ from pieces of surface entering or leaving at the boundary of V contribute negligibly in the limit of large V.

Now, the right-hand side of (43) is a homogeneous functional of degree -1 because if we dilate Γ by a factor α then $|V|^{-1}$ is multiplied by $\alpha^{-\nu}$ and the surface area by $\alpha^{\nu-1}$; therefore, by the lemma, the expectation $\langle\sigma(\Gamma(t))\rangle$ is proportional to $[h(t)]^{-1}$. Similarly, the right-hand side of (A2) is a homogeneous function of degree -4 because if we dilate Γ by a factor α, then the product of $|V|^{-1}$ and $\int_V dH(\Gamma)$ is multiplied by α^{-1} as before, κ is multiplied by α^{-1}, and v is multiplied by one factor α^{-1} arising from the gradient in (27) and a further α^{-1} arising from the factor κ in (28); therefore, by the lemma, the expectation $(d/dt)\langle\sigma(\Gamma(t))\rangle$ is proportional to $[h(t)]^{-4}$. Combining these last two results we obtain

$$\frac{d}{dt}\{[h(t)]^{-1}\} = \text{const}\times[h(t)]^{-4} \,. \tag{A3}$$

Solving this differential equation, we find that $[h(t)]^3$ must be a linear function of t, and then substitution into (42) completes the proof.

APPENDIX B: THE SCALING FUNCTION AT SMALL x

We start from the Cahn-Hilliard equation in the form (23), but with the symbol t_1 replaced by t for typographical reasons. Integration with respect to t gives

$$u^\epsilon(\mathbf{r},t)=u(\mathbf{r},0)-\nabla^2 y^\epsilon(\mathbf{r},t)\ , \tag{B1}$$

where

$$y^\epsilon(\mathbf{r},t)=\epsilon^{-1}\int_0^t \mu^\epsilon(\mathbf{r},t')dt'\ . \tag{B2}$$

Defining $\tilde{S}^\epsilon(\mathbf{k},t)$ to be the approximate structure function obtained by using u^ϵ in place of u_0 in the definition (6), and substituting from (B1) into that definition, we obtain

$$\tilde{S}^\epsilon(\mathbf{k},t)=\tilde{S}(\mathbf{k},0)-2\langle P^\epsilon(\mathbf{k},t)\rangle+\langle Q^\epsilon(\mathbf{k},t)\rangle\ , \tag{B3}$$

where we have defined

$$2P^\epsilon(\mathbf{k},t)=\lim_{|V|\to\infty}\left[|V|^{-1}\int_V [u^\epsilon(\mathbf{r},0)-\phi]e^{i\mathbf{k}\cdot\mathbf{r}}d^\nu\mathbf{r}\int_V \nabla^2 y^\epsilon(\mathbf{r},t)e^{-i\mathbf{k}\cdot\mathbf{r}}d^\nu\mathbf{r}+\text{c.c.}\right]\ , \tag{B4}$$

and

$$Q^\epsilon(\mathbf{k},t)=\lim_{|V|\to\infty}\left[|V|^{-1}\left|\int_V \nabla^2 y^\epsilon(\mathbf{r},t)e^{i\mathbf{k}\cdot\mathbf{r}}d^\nu\mathbf{r}\right|^2\right]\ . \tag{B5}$$

The Schwartz inequality applied to the definition of P^ϵ gives

$$|\langle P^\epsilon(\mathbf{k},t)\rangle|^2\le\tilde{S}(\mathbf{k},0)\langle Q^\epsilon(\mathbf{k},t)\rangle\ . \tag{B6}$$

To estimate $Q^\epsilon(\mathbf{k},t)$, which is the dominant term in (B3), we use Green's theorem in (B5). Since the surface terms do not contribute in the $V\to\infty$ limit, we obtain

$$k^{-4}\langle Q^\epsilon(\mathbf{k},t)\rangle=\lim_{|V|\to\infty}\left[|V|^{-1}\int_V\int_V\langle y^\epsilon(\mathbf{r},t)y^\epsilon(\mathbf{r}',t)\rangle e^{i\mathbf{k}\cdot(\mathbf{r}-\mathbf{r}')}d^\nu\mathbf{r}\,d^\nu\mathbf{r}'\right]\ , \tag{B7}$$

where k denotes the length of the vector $\mathbf{k}$. It is to be expected that $y^\epsilon(\mathbf{r},t)$ and $y^\epsilon(\mathbf{r}',t)$ will be uncorrelated if $|\mathbf{r}-\mathbf{r}'|$ is much greater than the length scale $k_m(t)^{-1}$, so that the right-hand side of (B7) will be close to its $|V|\to\infty$ limit by the time the diameter of V has reached a value $Ck_m(t)^{-1}$, where C is a constant depending on the definition of "close to" but not on t. Denoting by $V(t)$ the region V reached at this stage, we have from (B7)

$$\begin{aligned}k^{-4}\langle Q^\epsilon(\mathbf{k},t)\rangle&\simeq|V(t)|^{-1}\int_{V(t)}\int_{V(t)}\langle y^\epsilon(\mathbf{r},t)y^\epsilon(\mathbf{r}',t)\rangle e^{i\mathbf{k}\cdot(\mathbf{r}-\mathbf{r}')}d^\nu\mathbf{r}\,d^\nu\mathbf{r}'\\&\simeq|V(t)|^{-1}\int_{V(t)}\int_{V(t)}\langle y^\epsilon(\mathbf{r},t)y^\epsilon(\mathbf{r}',t)\rangle d^\nu\mathbf{r}\,d^\nu\mathbf{r}'\quad\text{for } k\ll C^{-1}k_m(t)\\&=|V(t)|^{-1}\left\langle\left[\epsilon^{-1}\int_0^t\left[\int_{V(t)}\mu^\epsilon(\mathbf{r},t')d^\nu\mathbf{r}\right]dt'\right]^2\right\rangle\quad\text{by (B2)}\ .\end{aligned} \tag{B8}$$

To estimate the integral over the region $V(t)$ in this last formula we divide the region into two parts. One part is a layer of thickness $O(\epsilon)$ near the interface $\Gamma(t')$; within it $\mu(t')$ is $O(1)$ and so the contribution of this part to the integral is of order $\epsilon\sigma(t')|V(t)|$, where $\sigma(t')$ is the surface area per unit volume at time t'. The other part of $V(t)$ is outside this surface layer; in this part, by (28) and the maximum principle for Laplace's equation, μ is of order $\epsilon\mu_1$, where μ_1 is of order $\tau\kappa=O(1)O(k_m(t'))$, and so the contribution of this part to the integral is of order $\epsilon k_m(t')|V(t)|$. Substituting these estimates into (B8) and using the estimate $\sigma(t)=O(k_m(t)^{-1})$, we obtain

$$k^{-4}\langle Q^\epsilon(\mathbf{k},t)\rangle\simeq\text{const}\times|V(t)|\left[\int_0^t k_m(t')dt'\right]^2\quad[k\ll C^{-1}k_m(t)]\ . \tag{B9}$$

In the limit of large t we have, by theorems (iii) and (iv) in Sec. IV C, $k_m(t')\sim\text{const}\times t^{-1/3}$ and so

$$\int_0^t k_m(t')dt'\sim\text{const}\times t^{2/3}\sim\text{const}\times[k_m(t)]^{-2}\ . \tag{B10}$$

Substituting this into (B9) and remembering also that $|V(t)|=\text{const}\times[k_m(t)]^{-\nu}$ we obtain

$$k^{-4}\langle Q^\epsilon(k,t)\rangle\simeq\text{const}\times[k_m(t)]^{-\nu-4}\quad[k\ll C^{-1}k_m(t)] \tag{B11}$$

where the constant is independent of both ϵ and t in the limit $\epsilon\to\infty$.

We can now estimate $F(x)$, starting from the formula (41). Using theorem (iii) in Sec. IV C we can rewrite this formula as

$$x^{-4}F(x)=\text{const}\times\lim_{t\to\infty}\{[k_m(t)]^{\nu+4}[xk_m(t)]^{-4}\tilde{S}(xk_m(t),t)\} \tag{B12}$$

and consider separately the contributions of the three terms of the expression (B3) for $\tilde{S}$. The term $\tilde{S}(\mathbf{k},0)$ depends on the initial conditions but will certainly have an upper bound independent of $\mathbf{k}$ and t. Since $k_m(t)\to 0$ as $t\to 0$, the contribution of this term to the right-hand side of (B12) vanishes. Because of (B11), the contribution of the Q term in (B3) to the right-hand side of (B12) is approximately constant for $x \ll C^{-1}$. The P term, by (B4), gives a contribution bounded above by the geometric mean of the other two, which is zero. So only the Q term survives and we obtain the desired result,

$$F(x)\simeq \text{const}\times x^4 \quad \text{for } x \ll C^{-1} . \tag{B13}$$

APPENDIX C: CALCULATION OF THE SCALING FUNCTION IN ONE DIMENSION FOR INDEPENDENT INTERVALS ON A LINE AS SHOWN IN FIG. 6

Let us denote by $p(l)dl$ the probability distribution for the interval length l with $\rho^{-1}=\int_0^\infty lp(l)dl$ and define $P_s(r)=\int_{r/s}^\infty p(l)dl$ for any $s>0$. We further denote by $q_n(r)$ the conditional probability that both ends A and B of a randomly thrown stick of length r are inside the black phase, given that A and B are located within the intervals 0 and n, respectively (see Fig. 6). The one-dimensional correlation function can then be written

$$g(r)=\sum_{n=0}^{\infty} q_n(r)-\phi^2 . \tag{C1}$$

1. Alternately colored intervals ($\phi=0.5$)

We find

$$\begin{aligned} &q_0(r)=(\rho/2)\int_r^\infty (l-r)p(l)dl , \\ &q_n\equiv 0 \quad \text{for } n \text{ odd} , \\ &q_n=(\rho/2)P_1 * p^{*(n-1)} * P_1 \quad \text{for } n \text{ even} , \end{aligned} \tag{C2}$$

where the asterisk denotes the convolution and p^{*n} means multiple convolution. Using this expression it is easy to calculate the Laplace transform of g in the form

$$\tilde{g}(s)=\phi(1-\phi)\left[\frac{1}{s}-\frac{2\rho}{s^2}\frac{1-\tilde{p}(s)}{1+\tilde{p}(s)}\right] , \tag{C3}$$

where $\tilde{p}$ denotes the Laplace transform of p. The Fourier transform $\hat{g}$ of $g(r)$ may then be calculated as $\hat{g}(k)=\tilde{g}(ik)+\tilde{g}(-ik)$, which, in case $p(l)$ representing a Poisson distribution, gives a Lorentzian with a maximum at $k=0$. In fact, for any distribution $p(l)$, $\hat{g}(0)=\rho(\int_0^\infty l^2 p(l)dl-\rho^{-2})$ is different from 0 (unless p is a δ function).

2. The black phase occupies a fraction ϕ of each interval located at the left side of the interval

In this case one obtains

$$\begin{aligned} &q_0(r)=\rho\int_{r/\phi}^\infty (\phi l-r)p(l)dl , \\ &q_n=\rho(P_1-P_{1-\phi})*p^{*n-1}*P_\phi \quad \text{for } n\neq 0 . \end{aligned} \tag{C4}$$

Consequently,

$$\tilde{g}(s)=\phi(1-\phi)\frac{1}{s}-\rho\frac{[1-\tilde{p}(\phi s)][1-\tilde{p}((1-\phi)s)]}{s^2[1-\tilde{p}(s)]} . \tag{C5}$$

In the case of a Poisson distribution the scaling function may be computed by normalizing the Fourier transform of g in the proper way:

$$F(x)=\frac{x^2}{[x^2(1-\phi)+\phi](x^2\phi+1-\phi)} , \tag{C6}$$

which is proportional to x^2 at small x.

3. The black phase occupies a fraction ϕ of each interval located in the center of the interval

We have

$$\begin{aligned} &q_0(r)=\rho\int_{r/\phi}^\infty (\phi l-r)p(l)dl , \\ &q_n=\rho(P_{(1+\phi)/2}-P_{(1-\phi)/2})*p^{*(n-1)}*(P_{(1+\phi)/2}-P_{(1-\phi)/2}) \quad \text{for } n\neq 0 , \end{aligned} \tag{C7}$$

and, consequently,

$$\tilde{g}(s)=\phi(1-\phi)\frac{1}{s}-\rho\frac{[1-\tilde{p}(\phi s)][1-\tilde{p}(s)]-(\tilde{p}\{[(1-\phi)/2]s\}-\tilde{p}\{[(1+\phi)/2]s\})^2}{s^2[1-\tilde{p}(s)]} . \tag{C8}$$

In the case of a Poisson distribution the structure function becomes

$$\hat{g}(k)=\rho\phi^2(1-\phi)^2\frac{(1+\phi)^2}{8}\frac{[7\rho^4+(1+2\phi^2)\rho^2k^2+\frac{1}{16}(1-\phi^2)^2k^4]}{\{\rho^2+[(1+\phi)/2]^2k^2\}^2\{\rho^2+[(1-\phi)/2]^2k^2\}^2(\rho^2+\phi^2k^2)}k^4 , \tag{C9}$$

which has the correct k^4 behavior at small k. Note that this result does not depend on the assumption of a Poisson distribution: one can show that $\hat{g}(k)\propto k^4$ (when $k\to 0$) holds for any interval length distribution $p(l)dl$. For a fixed volume fraction $\phi=0.5$, the scaling function has been calculated numerically for interval length distribution of the type

$$p_n(l)=\frac{n\rho}{\Gamma(n)}(n\rho l)^{n-1}e^{-n\rho l} \quad \text{with } n>1 \ , \tag{C10}$$

giving

$$\tilde{p}_n(s)=\left[1+\frac{s}{n\rho}\right]^{-n} , \tag{C11}$$

and the results are plotted in Fig. 7 for several values of n.

---

*Permanent address.

[1]J. D. Gunton, M. San Miguel, and P. S. Sahni, in *Phase Transitions and Critical Phenomena,* edited by C. Domb and J. L. Lebowitz (Academic, New York, 1983), Vol. 8.

[2]H. Furukawa, Adv. Phys. **34**, 703 (1985).

[3]*Dynamics of Ordering Processes in Condensed Matter,* edited by S. Komura and H. Furukawa (Plenum, New York, 1988).

[4]K. Binder, in *Materials Science and Technology,* edited by P. Haasen (VCH Verlagsges., Weinheim, 1991), Vol. 5, Chap. 7, p. 405.

[5]I. M. Lifshitz and V. V. Slyozov, J. Phys. Chem. Solids **19**, 35 (1961).

[6]W. W. Mullins and J. Viñals, Acta Metall. **37**, 991 (1989).

[7]Y. Enomoto and K. Kawasaki, Acta Metall. **37**, 1399 (1989).

[8]W. C. Johnson, T. A. Abinandanan, and P. W. Voorhees, Acta Metall. Mater. **38**, 1349 (1990); P. H. Leo, W. W. Mullins, R. F. Sekerka, and J. Viñals, *ibid.* **38**, 1573 (1990).

[9]P. Fratzl, F. Langmayr, G. Vogl, and F. Miekeley, Acta Metall. Mater. **39**, 753 (1991).

[10]A. G. Khachaturyan, S. V. Semenovskaya, and J. W. Morris, Jr., Acta Metall. **36**, 1563 (1988).

[11]G. Kostorz, J. Appl. Crystallogr. (to be published).

[12]J. Marro, J. L. Lebowitz, and M. H. Kalos, Phys. Rev. Lett. **43**, 282 (1979); J. L. Lebowitz, J. Marro, and M. H. Kalos, Acta Metall. **30**, 297 (1982); P. Fratzl, J. L. Lebowitz, J. Marro, and M. H. Kalos, *ibid.* **31**, 1849 (1983).

[13]P. Fratzl and J. L. Lebowitz, Acta Metall. **37**, 3245 (1989).

[14]C. Yeung, Phys. Rev. Lett. **61**, 1135 (1988).

[15]H. Furukawa, J. Phys. Soc. Jpn. **58**, 216 (1989).

[16]G. Porod, Kolloid-Zeitschrift **124**, 83 (1951); **125**, 51 (1952).

[17]G. Porod, in *Small-Angle X-ray Scattering,* edited by O. Glatter and O. Kratky (Academic, London, 1983).

[18]J. Marro, A. B. Bortz, and M. H. Kalos, Phys. Rev. B **12**, 2000 (1975); M. Rao, M. H. Kalos, J. L. Lebowitz, and J. Marro, *ibid.* **13**, 4328 (1976); A. Sur, J. L. Lebowitz, J. Marro, and M. H. Kalos, *ibid.* **15**, 3014 (1977).

[19]A. Chakrabarti, R. Toral, and J. D. Gunton, Phys. Rev. B **39**, 901 (1989).

[20]T. M. Rogers and R. C. Desai, Phys. Rev. B **39**, 11 956 (1989).

[21]K. R. Elder and R. C. Desai, Phys. Rev. B **40**, 243 (1989).

[22]O. Penrose, Rep. Prog. Phys. **42**, 1937 (1979).

[23]R. L. Pego, Proc. Roy. Soc. **422**, 261 (1989).

[24]P. de Mottoni and M. Schatzmann (unpublished).

[25]G. F. Mazenko, O. T. Valls, and M. Zanetti, Phys. Rev. B **38**, 520 (1988); G. F. Mazenko, Phys. Rev. Lett. **63**, 1605 (1989); Phys. Rev. B **43**, 8204 (1991).

[27]J. W. Cahn, Trans. Met. Soc. AIME **242**, 166 (1968).

[28]J. L. Lebowitz, E. Orlandi, and E. Presutti, J. Stat. Phys. (to be published).

[29]L. A. Santalo, *Integral Geometry and Geometric Probability* (Addison-Wesley, New York, 1976), Secs. 3.1 and 12.2.

[30]P. Debye, H. R. Anderson, and H. Brumberger, J. Appl. Phys. **28**, 679 (1957).

[31]M. Teubner and R. Strey, J. Chem. Phys. **87**, 3195 (1987).

[32]C. Roland and M. Grant, Phys. Rev. B **39**, 11 971 (1989).

[33]M. Suzuki, in *Dynamics of Ordering Processes in Condensed Matter* (Ref. 3), p. 23.

[34]J. J. Hoyt and D. de Fontaine, Acta Metall. **37**, 1611 (1989).

[35]P. Rikvold and J. D. Gunton, Phys. Rev. Lett. **49**, 286 (1982).

[36]J. G. Amar, F. E. Sullivan, and R. D. Mountain, Phys. Rev. B **37**, 196 (1988).

[37]J. G. Amar and F. Sullivan, Comp. Phys. Commun. **55**, 287 (1989).

[38]D. A. Huse, Phys. Rev. B **34**, 7845 (1986).

[39]S. M. Allen and J. W. Cahn, Acta. Metall. **27**, 1085 (1979).

[40]H. E. Cook, Acta. Metall. **18**, 297 (1970).

[41]W. W. Mullins, J. Appl. Phys. **59**, 1341 (1986).

[42]A. Guinier and G. Fournet, *Small-Angle Scattering of X-rays* (Wiley, New York, 1955).

[43]H. Furukawa, Phys. Rev. B **40**, 2341 (1989).

[44]L. A. Feigin and D. I. Svergun, *Structure Analysis by Small-Angle X-ray and Neutron Scattering,* (Plenum, New York, 1987), Chap. II.

[45]F. S. Bates and P. Wiltzius, J. Chem. Phys. **91**, 3258 (1989).

[46]A. Shinozaki and Y. Oono, Phys. Rev. Lett. **66**, 173 (1991).

[47]P. Fratzl, J. Appl. Crystallogr. (to be published).

[48]Y. Enomoto, M. Tokuyama, and K. Kawasaki, Acta Metall. **34**, 2119 (1986), and references cited therein.